JACS
JOURNAL OF THE AMERICAN CHEMICAL SOCIETY

Article

pubs.acs.org/JACS

New Basic Insight into Reductive Functionalization Sequences of Single Walled Carbon Nanotubes (SWCNTs)

Ferdinand Hof, Sebastian Bosch, Siegfried Eigler, Frank Hauke, and Andreas Hirsch*

Department of Chemistry and Pharmacy & Institute of Advanced Materials and Processes (ZMP), Friedrich-Alexander-Universität Erlangen-Nürnberg (FAU), Henkestrasse 42, 91054 Erlangen, Germany

Supporting Information

ABSTRACT: The reactivity of reduced single walled carbon nanotubes (SWCNTs) (carbon nanotubides), prepared under strict inert conditions in a glovebox with respect to the covalent functionalization with hexyl iodide and subsequent exposure to ambient conditions (air, moisture), was systematically investigated by Raman, absorption, fluorescence, and IR spectroscopy as well as by TG/MS measurements. We have discovered that the alkylation does not lead to a complete discharging of the tubes since follow-up reactions with moisture still take place leading to mixed functionalized carbon nanotube derivatives containing H- and OH-addends (but no carboxylates) next to the hexyl groups. This was confirmed by the exposure of carbon nanotubides to ambient conditions. The degree of hexylation determined both under strict inert (ic) and ambient (ac) conditions increases with an increasing K:C ratio of the reduced SWCNT starting material. The presence of OH-groups covalently attached to the nanotubes was also confirmed by postfunctionalization reactions with 2-thiophenecarbonyl chloride, leading to the corresponding esters. Control experiments with KO_2 give rise to the formation of the same oxygen functionalities. These combined findings allowed for the suggestions of a plausible reaction mechanism, describing all the observed reactions on the SWCNTs side walls. The amount of subsequent side reactions after the treatment of reduced SWCNTs with electrophiles is strongly influenced by the reduction potential of the electrophile, which is responsible for the extent of reoxidation. Incomplete quenching of negative charges allows stronger oxidants/electrophile (e.g., O_2) to perform follow-up reactions.

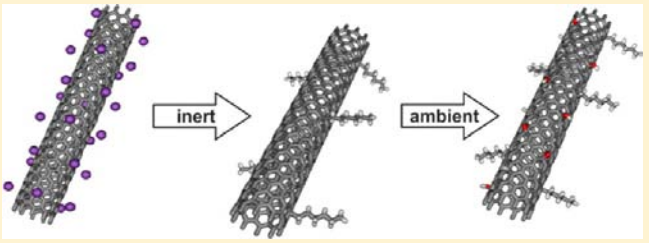

INTRODUCTION

The field of single walled carbon nanotube (SWCNT) chemistry has steadily developed during recent years, and a series of successful functionalization protocols have been reported.[1−7] Despite this encouraging evolution, many aspects of covalent SWCNT chemistry including electronic-type selectivity, regiochemistry, important side reactions, and also an unambiguous characterization of reaction products are not understood in detail.[8−10] Therefore, further systematic work to reveal such fundamental questions is urgently required. It turned out that the activation of the pristine nanotube starting material is a crucial step providing an efficient exfoliation of bundles and an effective addend binding. Here, negatively charged carbon nanotube anions—carbon nanotubides—serve as versatile and highly reactive species for subsequent sidewall addition reactions of electrophiles.[11,12] This reductive activation method has also been applied for functionalizing other carbon allotropes such as graphite[13−17] and fullerenes.[18−21] Carbon nanotubides can be produced *in situ* by either a nucleophilic addition of organometallic reagents[9,22−25] or by the application of Birch-type reaction protocols,[10,26,27] e.g., by the reduction with alkali metals in liquid ammonia. In either case, the charging of the carbon nanotubes is associated with a very efficient Coulomb driven exfoliation of the starting material leading to an increased solubility of the individualized species in organic solvents,[28−31] providing the basis for subsequent functionalization reactions. For instance, quenching of these negative charges accompanied by a covalent addend binding has been achieved, by the treatment of nanotubides with alkyl- and aryl-halides,[26,27] carbonyl compounds, i.e., ketones, esters,[6] and carbon dioxide[7] as well as diazonium salts.[32,33] Moreover, negative charging (n-type doping)[34−37] of SWCNTs has also a significant effect on the respective optoelectronic properties[38,39] and on the specific Raman characteristics of SWCNTs.[40,41]

In order to tackle the problem of a satisfactory characterization of covalently functionalized nanotube derivatives, we have recently introduced a very helpful tool, namely, statistical Raman spectroscopy.[33] This method allows the extraction of reliable information about the degree of functionalization, reaction selectivity and sample homogeneity. This bulk information is obtained by large area Raman mappings and analysis of a large data set of single point spectra by statistical methods. For example, an entire set of intensity ratios of the Raman D- and G-bands, $I_{D/G}$ values, indicative for the degree of functionalization, are plotted according to their frequency, which in many cases leads to a Gaussian-type distribution. The homogeneity of a given sample determined at a certain

Received: June 24, 2013
Published: November 20, 2013

   dx.doi.org/10.1021/ja4063713 | J. Am. Chem. Soc. 2013, 135, 18385−18395

wavelength can be expressed by the respective standard deviation ± ω of the corresponding Gaussian function.

In this report, we present a systematic and careful analysis of alkylated SWCNTs generated by the reaction of carbon nanotubides with hexyl iodide. The emphasis of this work lies in shining light on the reaction mechanism, the control of the functionalization efficiency and the detailed study of the reactivity of the intermediately formed carbon nanotubides with respect to various reaction conditions. We clearly demonstrate that working under strict inert gas conditions is a crucial prerequisite in order to exclude side reactions. Intermediate carbon nanotubides are very sensitive to moisture and atmospheric oxygen which can lead to the formation of oxygen functionalities in addition to alkyl chain binding. The combination of statistical Raman analysis and a systematic variation of the reaction conditions provide a deep insight into fundamental aspects of carbon nanotube reactivity, being of great value for future developments.

EXPERIMENTAL SECTION

Synthesis. In previous publications, potassium was used to establish n-type doped carbon nanotubides, where a maximum stoichiometry between KC_8 up to KC_{16} has been reached.[42−49] For the formation of highly reactive and individualized carbon nanotubides **B** we used molten potassium and HiPco tubes (Scheme 1). The metal/SWCNT mixture was heated for 6 h at 150 °C in an argon atmosphere (glovebox; <0.1 ppm oxygen, <0.1 ppm water). Variation of the potassium/carbon ratios lead to the formation of the carbon nanotubide salts $\mathbf{A_1}$−$\mathbf{A_6}$: $\mathbf{A_1}$ [K:C = 1:2], $\mathbf{A_2}$ [K:C = 1:4], $\mathbf{A_3}$ [K:C = 1:6], $\mathbf{A_4}$ [K:C = 1:10], $\mathbf{A_5}$ [K:C = 1:18], $\mathbf{A_6}$ [K:C = 1:100]. Depending on the stoichiometry, black (low potassium content, K:C = 1:100−1:10) or beige (high potassium content, K:C = 1:6, 1:4, 1:2) compounds were isolated. These salts were used for the subsequent functionalization processes.

For the solvent driven individualization of the carbon nanotubides the salts $\mathbf{A_1}$−$\mathbf{A_6}$ ($\mathbf{A_1}$−$\mathbf{A_5}$: 2 mmol SWCNTs, $\mathbf{A_6}$: 4 mmol SWCNTs) were dispersed under argon in 50 mL $THF_{(abs)}$ and treated with a tip sonicator for 5 min (100 J) yielding the corresponding dispersions $\mathbf{B_1}$−$\mathbf{B_6}$. The *n*-hexyl functionalized derivatives $\mathbf{C_1}$−$\mathbf{C_6}$ were obtained by the addition of 5 equiv/C *n*-hexyl iodide. For the investigation of the influence of oxygen and water the two samples with the highest metal content $\mathbf{B_1}$ [K:C = 1:2] and $\mathbf{B_2}$ [K:C = 1:4] were removed from the glovebox and cooled under ambient conditions to −10 °C. Subsequently, molecular oxygen was gently bubbled through the dispersion (1 h, flow: 75 mL/min − 0.2 mol O_2 per hour). The final work up was carried out by an aqueous phase extraction (50 mL H_2O/50 mL cyclohexane) followed by filtration and drying, yielding the reaction products $\mathbf{D_1}$ and $\mathbf{D_2}$. For further identification of the chemical nature of the attached oxygen functionalities in **D**, a coupling experiment has been carried out. For this purpose 22.0 mg of $\mathbf{D_1}$ was dispersed in 50 mL THF under inert gas atmosphere by the aid of a short tip ultrasonication treatment. Afterward, 791 mg (10.0 mmol) absolute pyridine and 1.46 g 2-thiophene carbonyl chloride (10.0 mmol) were added. The reaction mixture was removed from the glovebox and refluxed overnight. Subsequently, the final coupling product $\mathbf{E_1}$ was isolated after aqueous work up. The detailed outline of the conditions used for the synthesis of the different SWCNT derivatives is given in the Supporting Information (SI).

CHARACTERIZATION

UV−vis nIR and Fluorescence Spectroscopy. For the detailed characterization of the charged intermediately formed carbon nanotubides $\mathbf{B_5}$ and $\mathbf{B_6}$ (for details see SI) by absorption and emission spectroscopy, the corresponding supernatant of the carbon nanotubide dispersion (5 min sedimentation) was transferred into a 0.2 mL cuvette (1 cm path length) equipped with a screw cap and septum. The cuvette was additionally sealed with parafilm to maintain inert gas conditions after the transfer from the glovebox to the spectrometer and throughout the entire measurements.

Scheme 1. Formation of Carbon Nanotubides A Using Molten Potassium in Various Stoichiometries Followed by the Generation of Dispersed Carbon Nanotubides B and Subsequent Reaction with *n*-Hexyl Iodide to Provide Functionalized Tubes C[a]

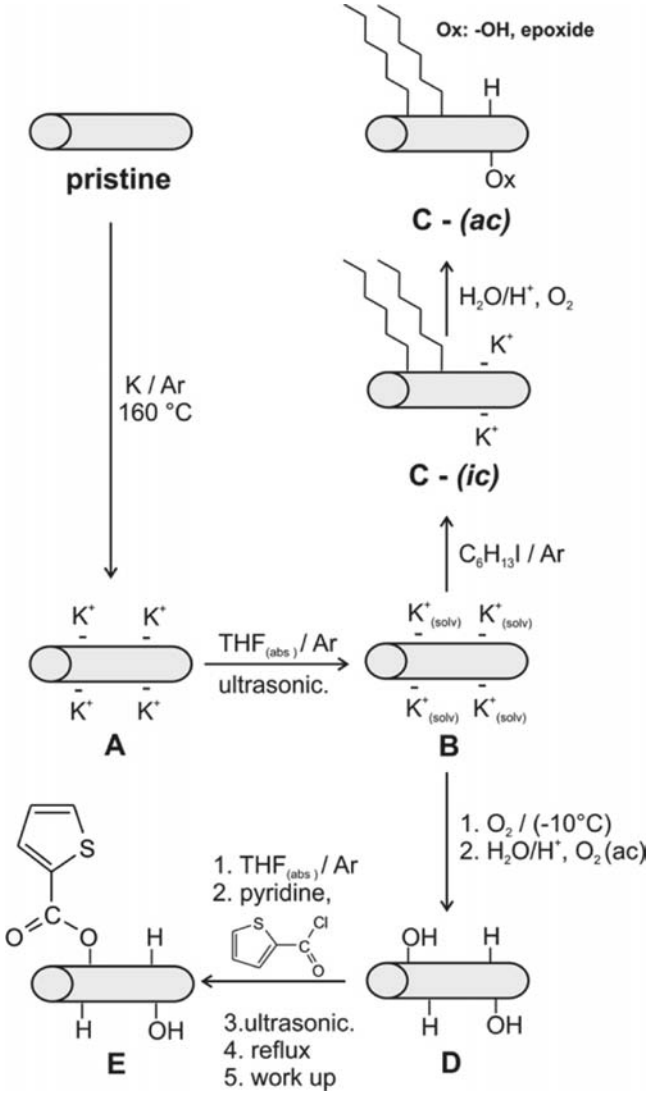

[a]Ambient conditions (ac) and inert gas conditions (ic). Exposure of carbon nanotubides **B** to molecular oxygen and ambient conditions (ac) leads to the formation of covalent adducts **D**. Post-functionalization of **D** yields thiophene coupled derivatives **E**.

Raman Analysis. For the Raman measurements under inert conditions (ic), the corresponding primary reaction products $\mathbf{C_1}$−$\mathbf{C_6}$ were filtered through a 0.2 μm reinforced cellulose membrane filter and washed with $THF_{(abs)}$ under argon. The corresponding nanotuby paper was subsequently placed between two glass slides and was air-tightly sealed with parafilm yielding samples $\mathbf{C_1^{ic}}$−$\mathbf{C_6^{ic}}$. For the reoxidation experiments the parafilm was removed, and the sample was exposed to ambient conditions (ac) leading to the formation of $\mathbf{C_1^{ac}}$−$\mathbf{C_6^{ac}}$. For the temperature-dependent Raman investigations 1 mL of the dispersion $\mathbf{C_1}$ was drop-casted onto a Si/SiO_2 wafer (300

dx.doi.org/10.1021/ja4063713 | J. Am. Chem. Soc. 2013, 135, 18385−18395

nm oxide layer). After the evaporation of the solvent in the glovebox, a film of *n*-hexyl functionalized carbon nanotubes was obtained. The wafer was removed from the glovebox and washed two times with purified water (5 mL each).

TG/MS Characterization. For the mass spectrometric coupled thermo gravimetric characterization (TG/MS) the dispersion $\mathbf{C}_1^{ac}$ was removed from the glovebox and transferred to a separation funnel containing cyclohexane and water (50 mL each). The water/THF phase was discarded, and the cyclohexane layer with the *n*-hexyl functionalized nanotubes was purged three times with water. Afterward, the organic layer was filtered through a 0.2 μm reinforced cellulose membrane filter and washed with 100 mL of THF. The functionalized derivatives were then scraped off the filter paper, and the resulting black powder was dried at RT in vacuum.

IR Spectroscopic Characterization. For IR measurements under inert conditions (ic), a ZnSe window was coated with the dispersion of $\mathbf{C}_2^{ic}$ in the glovebox, and the resulting film was dried in the glovebox. Subsequently, the film was washed with $THF_{(abs)}$, and the solvent was evaporated. Afterward, the ZnSe window was transferred into a glass vial, sealed with a screw cap, and removed from the glovebox. The IR spectroscopic characterization was carried out in an argon flooded (30 min argon purging) measuring chamber.

RESULTS AND DISCUSSION

Potassium Carbon Nanotubide Salts A. In a first step, samples, prepared *via* the solid-state reduction procedure described above, have been compared with the respective reference material obtained by potassium vapor doping published by the group of Smalley.[50] They monitored the SWCNT charging process in sealed quartz ampules by Raman spectroscopy and observed that the spectra have changed dramatically due to the n-type doping of the SWCNTs. Besides a charge-based damping[41,51] of all Raman modes they detected a pronounced low-energy shift of the G-band. For our Raman *in situ* studies, which had to be carried out in an inert gas environment (ic), samples were embedded between two glass cover slides and air tightly sealed by parafilm. With this setup, the successful reductive activation of the SWCNTs can quickly and easily be monitored by Raman spectroscopy (Figure S1). For instance, the respective Raman spectrum of the solid-state reduced SWCNT material $\mathbf{A}_2$, with the stoichiometry of [K:C = 1:4], is in perfect agreement with the vapor doping results[50] and therefore a clear indication for the generation of charged $SWCNT^{n-}$ intermediates.

Carbon Nanotubide Dispersions B. It has been demonstrated that reduced and exfoliated carbon nanotubes are most promising intermediates for subsequent functionalization reactions.[6,7,26,27,32] In order to monitor the long-term stability of carbon nanotubides and to investigate the influence of the charging step on the spectral features, we carried out a series of *in situ* UV−vis nIR studies (Figure 1). In contrast to the negatively charged carbon nanotubides, pristine HiPco tubes are completely insoluble in THF after the same ultrasonic treatment conditions (Figure S2). This illustrates the influence of the Coulomb driven exfoliation and the charge mediated stabilization of exfoliated carbon nanotubide dispersions. Furthermore, by a direct comparison of $\mathbf{B}_6$ [K:C = 1:100] and $\mathbf{B}_5$ [K:C = 1:18] (Figure S2) it becomes evident that the amount of charge has a direct influence on the dispersibility of the SWCNTs. The net carbon uptake, expressed by the measured absorbance, is lower in the case of $\mathbf{B}_6$ (Figure 1a) in contrast to $\mathbf{B}_5$ (Figure 1d) where a higher amount of potassium (factor of 6.1) has been used for the charging of the nanotubes. In a concentration-dependent study we determined this maximum carbon uptake of the nanotubide salt $\mathbf{B}_6$ with about 1.0 mg/mL (for detailed information see Figure S3). Moreover, our data lead to the conclusion that a linear uptake of charged SWCNTs is only fulfilled in a very low concentration regime.

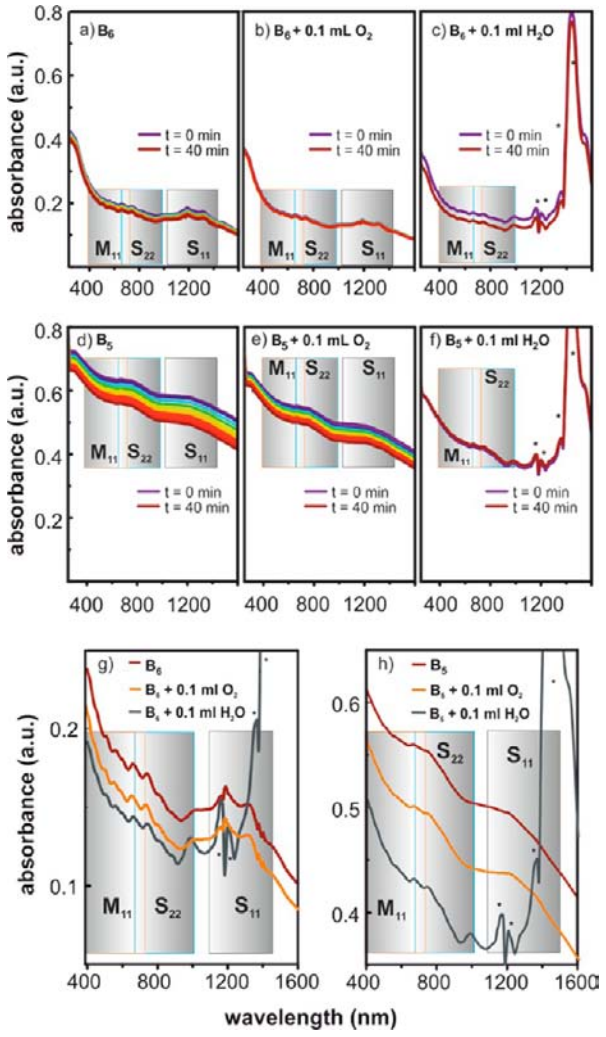

Figure 1. (a,d) Time-dependent *in situ* UV−vis nIR studies of the intermediately formed carbon nanotubides with varying potassium amount $\mathbf{B}_6$ and $\mathbf{B}_5$, dispersed, in THF. (b,e) Spectral changes after treatment with oxygen or (c,f) after treatment with water. (g,h) Magnification of the respective excitonic transition regions M_{11}, S_{22}, and S_{11}.

The amount of the applied charge has also a direct influence on the UV−vis nIR excitonic transitions, being related to the van Hove singularities in the density of states of the SWCNTs. In the lower charged carbon nanotubides $\mathbf{B}_6$ the respective transition bands can clearly be identified (Figure 1g), whereas the higher charged material $\mathbf{B}_5$ exhibits a clearly reduced spectral fine structure (Figure 1h). This can be explained by the continuous filling of unoccupied SWCNT states (conduction band) by electrons during the reduction process (Figure S4). It should be kept in mind that HiPco SWCNTs intrinsically exhibit a broad distribution of different electronic types and that the exact filling of a given chirality will depend on the band structure of the respective carbon nanotube. The absorption

dx.doi.org/10.1021/ja4063713 | J. Am. Chem. Soc. 2013, 135, 18385−18395

spectroscopy-based observation is supported by the data obtained from emission studies of $\mathbf{B_6}$ and $\mathbf{B_5}$ (Figure S5). Here, fluorescence from individualized semiconducting carbon nanotubides (λ_{exc} = 660 nm in S_{22}, emission from S_{11}) can be detected in $\mathbf{B_6}$ [K:C = 1:100] but not any longer in the case of $\mathbf{B_5}$ [K:C = 1:18]. It should be mentioned that SWCNT bundling could in principle yield the same spectroscopic results: loss of excitonic fine structure in absorption spectroscopy and loss of SWCNT nIR emission.[25] Nevertheless, in our opinion it has to be expected, that in higher negative charged systems the respective Coulomb driven exfoliation should yield better stabilized individual SWCNT species than in the case of systems equipped with a lower charge density. Therefore, for $\mathbf{B_6}$ bundled SWCNT aggregates are more likely than for $\mathbf{B_5}$. We therefore tend to attribute the observed spectral changes to the circumstance of an electronic filling of the conduction bands than to a simple aggregation phenomenon. This is corroborated by the fact, that bundled SWCNTs should sediment faster than individualized species. In time-dependent absorption studies (0−40 min) of the carbon nanotubide intermediates $\mathbf{B_6}$ and $\mathbf{B_5}$ (Figure 1a,d) we observed a long-term stability with no changes in respect to the spectral fine structure in both cases. The decrease of the overall absorption intensity measured at 660 nm can be calculated with about 9.3% and 12.3%, respectively, throughout this time span.

In order to evaluate the possibility of side reactions of carbon nanotubides during the aqueous work up, we investigated the influence of molecular oxygen and water on these charged intermediates. For this purpose, we added a huge molar excess of air and after 40 min a huge molar excess of water (0.1 mL each, both by gas tight Hamiltonian syringe injection) to the respective THF dispersion (0.2 mL) of $\mathbf{B_6}$ and $\mathbf{B_5}$ and measured the time-dependent changes of the corresponding absorption spectra (Figure 1b,e). The respective spectra of the oxygen treated SWCNT dispersion indicate that the charged SWCNTs were not completely reoxidized by this oxygen treatment, as the transfer of electrons would result in a discharging of the SWCNTs and thereforein either a restoration of all characteristic absorption features or a complete bundling and precipitation of the SWCNT material.

In our case, the exposure to oxygen does not lead to any significant spectral restoration, which implies only minor changes of the doping level of the carbon nanotubides expressed by only a marginal change in the optical density (Figure 1g,h). This situation changes drastically when water is added to $\mathbf{B_6}$ and $\mathbf{B_5}$ (Figure 1c,f), respectively. Here, in both cases the characteristic excitonic transitions are partially restored. This indicates that the overall level of doping is lowered by the addition of H_2O, and additionally this can be interpreted as a complete charge compensation. One should also bear in mind that a partial covalent sidewall functionalization would also yield similar UV−vis nIR absorption spectra, which has recently been demonstrated.[7] The discharging of the SWCNTs accompanied by the restoration of the pristine starting material without additional sidewall functionalization seems unlikely, because otherwise a precipitation of the SWCNT material, should be detected in Figure 1c,f.

For the stabilization of the negatively charged carbon nanotubide intermediates the choice of the right solvent is of fundamental importance. In general, it is desirable that the solvent is chemically inert with respect to any possible side reactions and that the polarity of the solvent efficiently assists in the debundling process. In principle, DMSO represents such a suitable candidate but, as has already shown by other authors,[52] also leads to the formation of a functionalized SWCNT material with methyl addends and sulfur-containing moieties.

Indeed, based on our charging experiments, we are able to confirm that DMSO is not an inert solvent in the presence of charged $SWCNT^{n-}$ species. For this purpose carbon nanotubides were dispersed in $DMSO_{abs}$ and THF_{abs}, respectively, by a short ultrasonic treatment (5 min/100 J) and the dispersed material was subsequently isolated by decantation and filtration without any exposure to ambient conditions. In order to gain statistically significant bulk information about a possible covalent functionalization of carbon nanotubides by the reaction with the respective solvent, 10 000 Raman spectra were recorded and the respective $I_{D/G}$ values (intensity ratios of the D- and G-bands) span up histograms exhibiting Gaussian type distributions (Figure 2a).

In contrast to the dispersion prepared in THF_{abs} ($\mathbf{B_2}$-THF) with a statistical $I_{D/G}$ value of 0.09 the sample dispersed in $DMSO_{abs}$ ($\mathbf{B_2}$-DMSO) exhibits a 2-fold increased $I_{D/G}$ value of 0.18, which implies a significant increase of addend bearing sp^3 framework atoms, based on a covalent sidewall addition

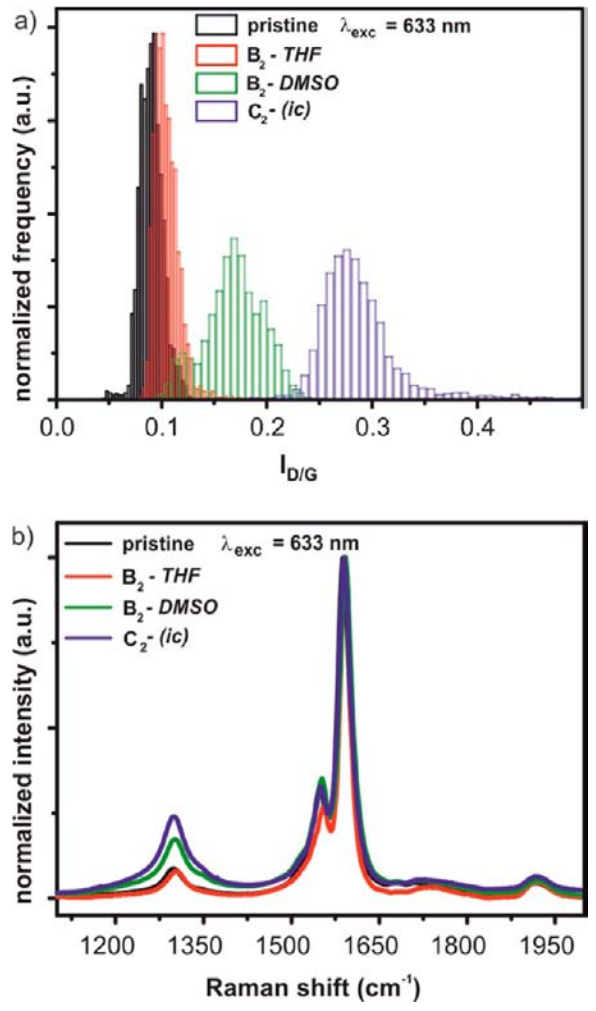

Figure 2. (a) Normalized frequency of the $I_{D/G}$ values (λ_{exc} = 633 nm) of the carbon nanotubide salt $\mathbf{A_2}$ dispersed in two different solvents THF ($\mathbf{B_2}$-THF) and DMSO ($\mathbf{B_2}$-DMSO). For comparison, $\mathbf{C_2}$ represents the alkylated material ($I_{D/G}$ = 0.29) after the addition of *n*-hexyl iodide to $\mathbf{B_2}$-THF. (b) Median spectra of the three samples based on their Gaussian distributions.

dx.doi.org/10.1021/ja4063713 | J. Am. Chem. Soc. 2013, 135, 18385−18395

reaction. This increase in the D-band intensity becomes also apparent by displaying the respective median spectra (Figure 2b). These results are also corroborated by the TG/MS characterization of the DMSO treated material (Figure S6). Here, we detected a significant mass loss of 15% (7% in the pristine starting material) and the characteristic mass fragments of covalently attached DMSO. Therefore, the conclusion can be drawn that in contrast to DMSO, THF represents a suitable and inert solvent for highly reactive carbon nanotubides.

Carbon Nanotubide Reactions C. As a reference system for the investigation of the chemical reactivity of carbon nanotubides we used hexyl iodide as trapping electrophile (Scheme 1). Therefore, the reactivity of the carbon nanotubides $\mathbf{A_2}$ (stoichiometry of [K:C = 1:4]) is discussed exemplarily in more detail. The respective potassium salt was dispersed in 10 mL THF_{abs} yielding $\mathbf{B_2}$. Afterward, 1.06 mL (5.00 mmol) *n*-hexyl iodide was added, and after 1 h stirring the functionalized SWCNT material $\mathbf{C_2^{ic}}$ was isolated under argon. Based on an *in situ* Raman analysis under inert gas conditions (Figure 3), we were able to prove the successful functionalization of the SWCNTs. Here, a mean $I_{D/G}$ value of 0.29 is obtained for the material after the addition of *n*-hexyl iodide.

Subsequently, the same sample was exposed to ambient conditions (ac) leading to the formation of $\mathbf{C_2^{ac}}$, where the respective mean $I_{D/G}$ value of 0.47 is increased by 61%. This overall increase of the $I_{D/G}$ value is a direct indication for an additional covalent sidewall functionalization, related to the exposure of the sample $\mathbf{C_2^{ic}}$ to atmospheric oxygen and moisture leading to the formation of side products.

This observation allows the conclusion that the treatment of the carbon nanotubide intermediate $\mathbf{B_2}$ with *n*-hexyl iodide did not lead to fully discharged carbon nanotubes. Therefore, anionic carbon nanotubides with a certain amount of negative charge still remain in the reaction mixture. These remaining charges can then subsequently initiate the reaction of carbon nanotubes with oxygen/moisture, finally leading to the formation of covalently bound oxygen and hydrogen functionalities. This observation is also fully consistent with the data obtained by the respective UV−vis nIR studies (see Figure 1).

In order to get a closer view on the underlying reaction principles and to investigate the influence of the amount of charge transferred to the carbon nanotubes, we prepared carbon nanotubide salts with varying potassium concentration $\mathbf{C_1^{ic}}$−$\mathbf{C_6^{ic}}$ [K/C=1:2−1:100]; all other parameters were kept constant. The mean $I_{D/G}$ values of the different samples with varying potassium content, extracted from the respective Gaussian distribution functions (Figures S7−S11) of the Raman maps, are depicted in Figure 4 (blue trace). The degree of functionalization exhibits a linear correlation with the potassium content in the range up to 1:2 ($\mathbf{C_1}$) and therefore the charging—doping level—of the SWCNTs. The slope of the regression line is experimentally found to be 0.95 and the *y*-axis intercept 0.08, representing the $I_{D/G}$ value of the starting material. After every measurement under inert gas conditions the respective sample was exposed to ambient conditions ($\mathbf{C_1^{ac}}$−$\mathbf{C_6^{ac}}$), and exactly the same area was mapped again.

If one would anticipate that the addition of *n*-hexyl iodide leads to a quantitative charge neutralization in terms of a single electron transfer from the carbon nanotubides to the electrophile, followed by a radical recombination[3,4,10] step, no further increase of the corresponding $I_{D/G}$ values after the

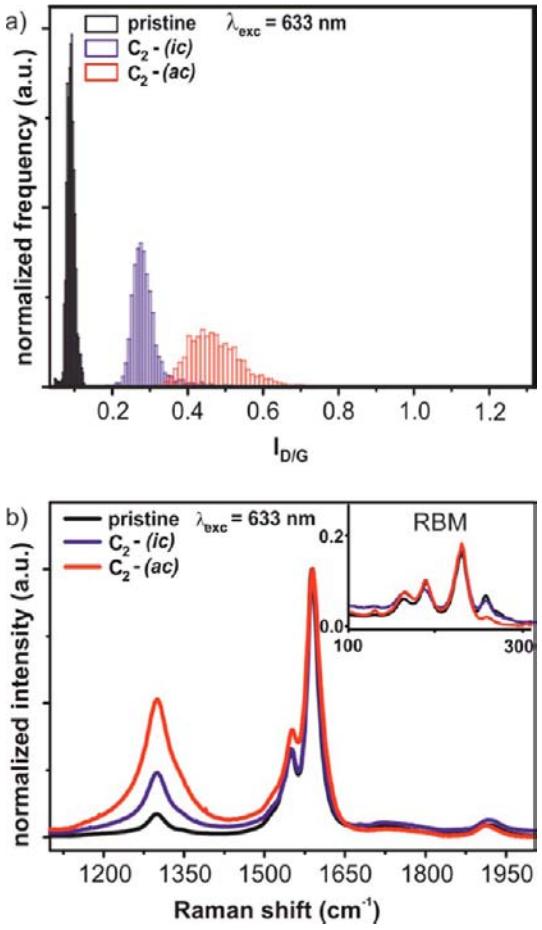

Figure 3. (a) Statistical Raman survey of $\mathbf{C_2^{ic}}$ and $\mathbf{C_2^{ac}}$ (λ_{exc} = 633 nm) under inert gas conditions (ic) and after exposure to ambient condition (ac). The same sample spot is probed in both cases. (b) Median spectra with the respective radial breathing mode (RBM) regions (inset).

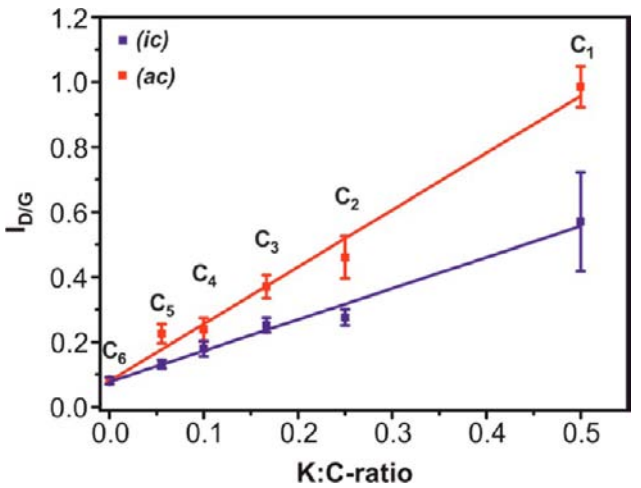

Figure 4. Intensity ratios of the Raman D- and G-bands ($I_{D/G}$ values) of $\mathbf{C_1^{ic}}$−$\mathbf{C_6^{ic}}$ and $\mathbf{C_1^{ac}}$−$\mathbf{C_6^{ac}}$ as a function of the ratio of potassium per carbon; a total of 5000 Raman spectra were recorded for each area (λ_{exc} = 633 nm). The measurements were performed under inert gas conditions (ic, blue trace) and subsequently under ambient conditions (ac, red trace).

dx.doi.org/10.1021/ja4063713 | J. Am. Chem. Soc. 2013, 135, 18385−18395

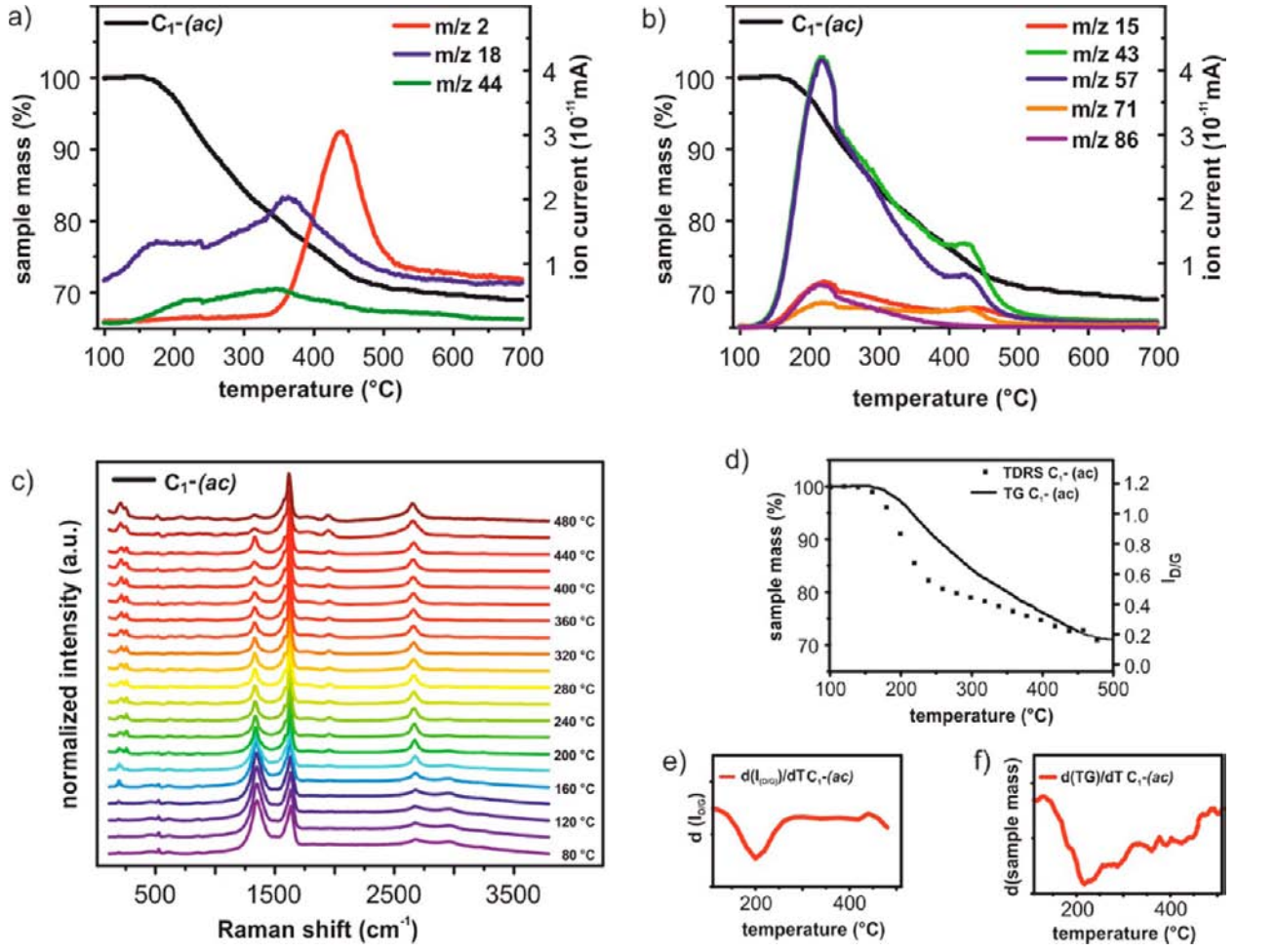

Figure 5. (a,b) Mass spectrometric coupled thermo gravimetric analysis (TG/MS) and (c) temperature-dependent Raman spectroscopy. (d) Comparison of TG derived sample mass loss and TDRS determined $I_{D/G}$ decrease. (e) First-order derivatives of the corresponding $I_{D/G}$ values and (f) corresponding mass loss of the hexyl functionalized sample $\mathbf{C}_1^{ac}$.

exposure to ambient conditions can be expected. However, the clearly increased $I_{D/G}$ values of $\mathbf{C}^{ac}$ compared with $\mathbf{C}^{ic}$ can be taken as an indication for a subsequent covalent functionalization of the hexyl derivatized SWCNTs with exposure to ambient conditions. Furthermore, our reference experiments have revealed that this $I_{D/G}$ increase is based on the sample exposure to ambient conditions and is not caused by laser induced damaging of the sp^2 lattice structure, as $\mathbf{C}^{ac}$ and $\mathbf{C}^{ic}$ behave differently. To answer the questions concerning the chemical nature of all covalently bound addends, we performed mass spectrometry coupled thermo gravimetric analysis (TG/MS) in combination with a novel setup for temperature depending Raman spectroscopy[53] (TDRS), see Figure 5. In carbon allotrope analytics, TG and TDRS represent two very useful and complementary techniques for the investigation of the temperature induced cleavage of covalently bound addends. Moreover, the TG/MS coupling setup provides further information on the chemical nature of the detached moieties. In the following, the analytical results obtained by the comparison of the respective TG/MS and Raman data (Figure 5) are exemplarily discussed on the basis of $\mathbf{C}_1^{ac}$ which is the product with the highest $I_{D/G}$ ratio (for comparison, the respective temperature-dependent Raman spectra of the pristine starting material can be found in Figure S12). For a direct comparison, the temperature-dependent Raman experiments were carried out under inert gas conditions and with the same heating rate, which has been used for the TG/MS measurements. In Figure 5a,b sample mass loss is plotted versus the respective mass traces of the following fragments: m/z 2 (H_2), 18 (H_2O), 44 (CO_2), 15, 43, 57, 71, 86 (hexyl fragments). The temperature-dependent Raman spectra are depicted in Figure 5c. By a direct comparison of the first-order derivative ($d(TG)/dT$ and $d(I_{D/G})/dT$) plots (Figure 5e,f) the peak flux of the functional group detachment can be determined at around 220 °C. This perfectly coincides with a maximum of the ion current of the respective hexyl chain fragments (m/z 15, 43, 57, 71, 85) depicted in Figure 5b. Remarkably, the temperature-dependent plot of the TG graph nicely correlates with the extracted $I_{D/G}$ values for every temperature (Figure 5d) and is based on the thermal detachment of the covalently bound hexyl chains. Encouraged by these results, we have checked if this correlation between two complementary analytical techniques can be generalized. Therefore, all samples $\mathbf{C}_1^{ac}$–$\mathbf{C}_6^{ac}$ were investigated by TG/MS analysis and scanning Raman spectroscopy. The respective mass loss profiles and the ion currents of the mass traces m/z 57 and m/z 86 (hexyl chain fragments) are depicted in Figure S13. The peak flux of detached hexyl moieties is detected in the region between 150 and 350 °C, and the sample mass loss in this region is correlated with the corresponding $I_{D/G}$ ratio of the

dx.doi.org/10.1021/ja4063713 | J. Am. Chem. Soc. 2013, 135, 18385−18395

respective sample (Figure S14a). In addition, we extracted the ion current intensity at the ion current flux maximum (220 °C) and correlated the respective data with the corresponding $I_{D/G}$ ratio (Figure S14b). For both mass traces we obtained a linear correlation between the respective TG/MS results and the Raman $I_{D/G}$ data. We have shown in a reference experiment, that oxidatively treated carbon nanotubes do not display a decrease of the respective $I_{D/G}$ ratio in TDRS (Figure S15). This temperature-dependent Raman study clearly proves that the reversible detachment of the covalently bound moieties does result in a rehybridization of sp^3 carbon atoms into sp^2 configuration and a restoration of the intact lattice structure of the carbon nanotubes. The defect induced D-band has almost completely vanished at a temperature of 480 °C, which is a clear indication for the reversible nature of the covalent sidewall functionalization of SWCNTs. In addition to the detection of hexyl chain fragments, the evolution of hydrogen, water, and carbon dioxide with the typical mass fragments (m/z 2, 18, 44) throughout the whole temperature region, starting from 150 °C up to 700 °C was monitored. The temperature-based evolution of CO_2 is an intrinsic carbon nanotube feature, detected throughout all samples (Figure S16).

Therefore, the detection of hydrogen and water leads to the conclusion that after the exposure to ambient conditions, an additional sidewall derivatization takes place resulting in mixed functionalized SWCNT derivatives $\mathbf{C}^{ac}$ with subsequently bound hydrogen and oxygen functionalities.

To further elucidate the chemical nature of these oxygen-containing functional groups, we have exposed $\mathbf{C}_1^{ac}$ (nanotuby paper) to hydrazine vapor and subsequently heated the system to 100 °C for 5 min. Hydrazine is a well-known reducing agent for graphene oxide and does very efficiently remove oxygen-containing addends such as epoxy functionalities.[54,55] In our case, the applied temperature does not lead to a structural degradation of the SWCNT material as an initial mass loss can only be detected starting at temperatures around 150 °C. Again, a detailed Raman investigation of the material was carried out after the treatment with hydrazine. As can clearly be seen from the plots of the Gaussian distribution function (Figure S17), the mean $I_{D/G}$ value of the hydrazine treated material has decreased by around 0.1, which is an indication for a partial lattice atom rehybridization to sp^2. We have also carried out a reference experiment with pristine SWCNTs. Here, the treatment with hydrazine does not lead to any changes. We therefore conclude that the hydrazine treatment of mixed functionalized SWCNT samples containing oxygen functionalities does lead to a partial defunctionalization.

This observation is also corroborated by an in-depth IR spectroscopic study of the mixed functionalized material (Figure 6). For this purpose a film of $\mathbf{C}_2^{ic}$ on a ZnSe window was prepared under an argon inert gas atmosphere. The subsequent IR measurements were also carried out under argon (Figure 6, blue trace). In this material, the IR active modes at 2929 and 2887 cm^{-1} can be assigned to C−H vibrations. The respective absorption bands in the region between 1250 and 1110 cm^{-1} are an indication for lattice vibrations of the carbon nanotubes. In this solely hexyl group functionalized material no vibrational bands indicative for oxygen-containing groups can be detected. Subsequently, this film was exposed to ambient conditions. The resulting sample $\mathbf{C}_2^{ac}$ (Figure 6, red trace) exhibits now a broad band at 3400 cm^{-1} and additional vibrational bands at 1595, 1396, and 1350 cm^{-1}.

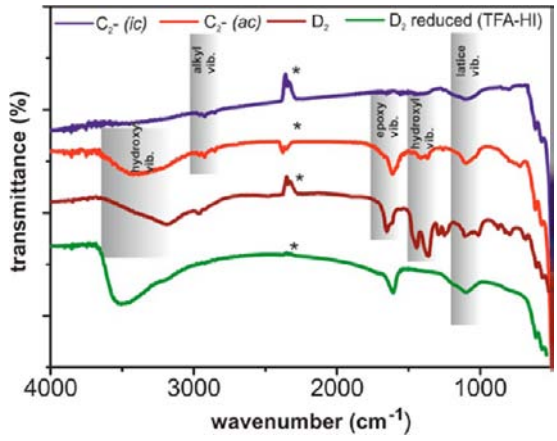

Figure 6. IR spectroscopic study of the samples $\mathbf{C}_2^{ic}$ and $\mathbf{C}_2^{ac}$ depicting the stepwise reaction pathway. For comparison a reference spectrum of $\mathbf{D}_2$ and the spectrum of reduced material is shown.

For an assignment of these new IR active bands we have prepared a reference sample $\mathbf{D}_2$ (brown trace) by the reaction of carbon nanotubides $\mathbf{B}_2$ with molecular oxygen (−10 °C, 1 h, 75 mL/min) followed by an aqueous work up (see Scheme 1). The absorption bands of this oxidatively treated material nicely coincide with the bands found for $\mathbf{C}_2^{ac}$. Treatment of this sample with hydroiodic acid (HI) and trifluoroacetic acid (TFA), which are known to remove hydroxyl groups on functionalized carbon allotropes,[56] lead to the disappearance of the IR active vibrations around 1450 cm^{-1} ($\mathbf{D}_2$, green curve). The IR vibrations at 3500 and 1610 cm^{-1} correspond to the iodine species,[57−59] which are adsorbed at the SWCNT sidewalls after the functionalization procedure and cannot be removed even at 250 °C. These conclusions are also confirmed by an in-depth Raman and TG/MS analysis of the reference sample $\mathbf{D}_2$ (see Figure 7).

As shown in Figure 7a, the direct treatment of carbon nanotubides with oxygen, followed by an aqueous work up, leads to an increase of the mean $I_{D/G}$ value from initially 0.08 ($\mathbf{B}_2$) to 0.28 ($\mathbf{D}_2$). In the respective TG/MS profile (Figure 7b), no evolution of carbon dioxide—indicative for an oxidative hole formation in the sp^2-framework—can be detected throughout the whole temperature regime. As already stated above, THF represents an appropriate inert solvent for the dispersion of carbon nanotubides. This is also true in the presence of molecular oxygen, as no side-product formation (absence of m/z 72 (THF), m/z 15 (CH_3), and no other fragments in the respective bar-graph spectra, (see Figure S18a) were detected. For $\mathbf{D}_2$ we obtained an overall mass loss of 8% accompanied by the detection of m/z 18 (H_2O) and m/z 17 (OH) indicative for the thermal detachment of covalently bound oxygen functionalities, i.e., covalently attached hydroxyl groups or ethylene oxides. Based on the observed mean $I_{D/G}$ value and on the respective sample mass loss, the degree of functionalization in $\mathbf{D}_2$ is comparable with the amount of functional entities installed by the reductive hexylation of carbon nanotubides in the case of $\mathbf{C}_2$. This reaction of oxygen with carbon nanotubes does only take place after the initial SWCNT charging as can be concluded from the respective reference experiment where uncharged SWCNTs have been treated under the same reaction conditions.

In this reference material exactly the same mass loss as in pristine HiPco SWCNTs was detected (Figure S18b).

dx.doi.org/10.1021/ja4063713 | J. Am. Chem. Soc. 2013, 135, 18385−18395

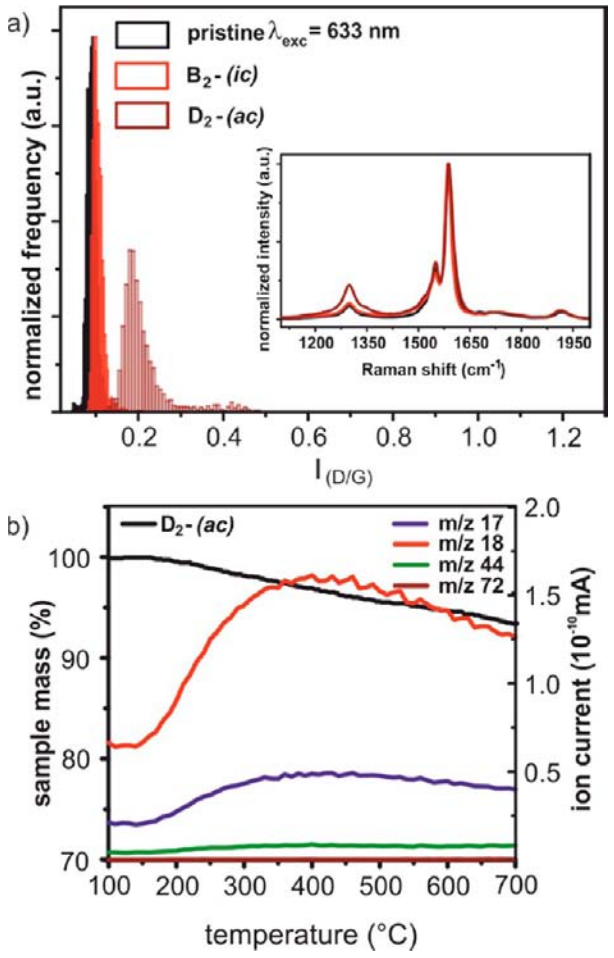

Figure 7. (a) Statistical Raman analysis (λ_{exc} = 633 nm) and median spectrum of the corresponding sample (inset). (b) TG/MS analysis of the oxygen functionalized sample $\mathbf{D_2}$.

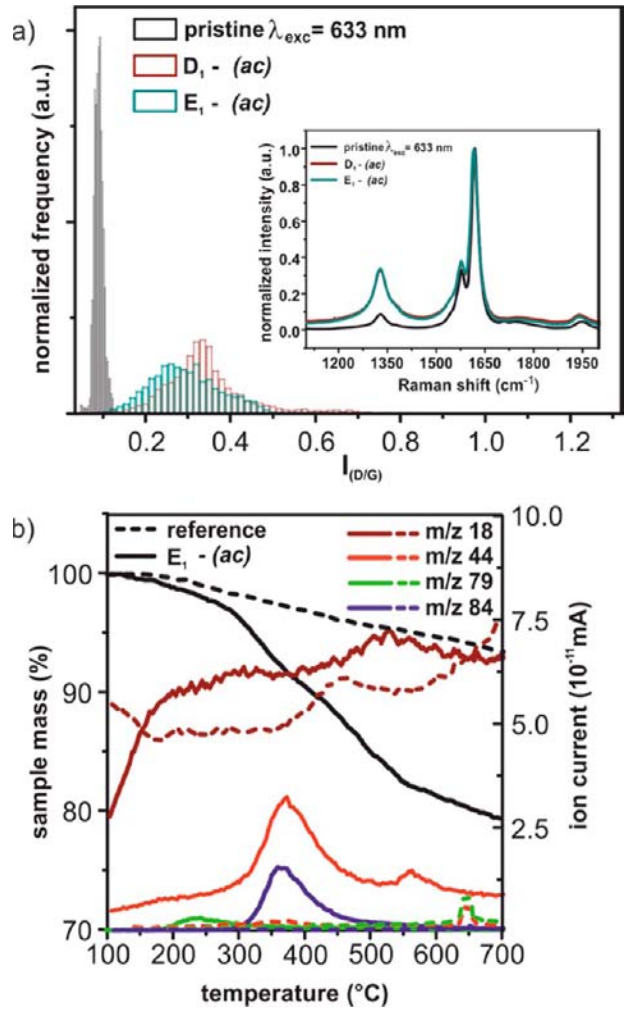

Figure 8. (a) Statistical Raman analysis (λ_{exc} = 633 nm) of $\mathbf{D_1}$ and of the coupling product $\mathbf{E_1}$. (b) TG-MS analysis of the thiophene derivatized sample $\mathbf{E_1}$.

Furthermore, we have no indication for the detachment of H_2O or OH in this material.

In principle, hydroxyl groups containing functionalized SWCNTs serve as a versatile platform, which can be addressed chemically under various conditions. The reaction with acyl chlorides is a well established sequence to address these groups. In order to substantiate the presence of hydroxyl groups covalently attached to the SWCNT scaffold, $\mathbf{D_1}$ was treated with 2-thiophenecarbonyl chloride under basic conditions yielding $\mathbf{E_1}$. Based on the obtained Raman data (Figure 8a) this secondary functionalization step has no influence on the original sp^2/sp^3 carbon ratio. However, in the corresponding TG/MS experiment (Figure 8b) the expected mass fragments for a thiophene carboxy moiety (m/z 44, 79, 84) can be detected at a temperature of 350 °C.

This observation can be explained by an ester formation and is corroborated by the fact that the ion current intensity of m/z 18 is decreased. In addition, the respective IR spectra do not exhibit any OH-based vibronic bands (Figure S19). In a reference experiment pristine SWCNTs were treated under the same conditions with 2-thiophenecarbonyl chloride. In the corresponding TG/MS-based analysis no indication for an attachment of a thiophene moiety could be found. These successful coupling experiments prove the initial sidewall hydroxylation of the SWCNTs during the aqueous work up. In an additional reference experiment THF dispersed pristine HiPco SWCNTs were treated with potassium superoxide in the presence of 18-crown-6 (Scheme 2).

Scheme 2. Reaction of Neutral HiPco SWCNTs with Potassium Superoxide Yielding Sidewall Hydroxylated SWCNTs

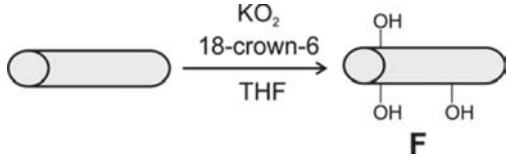

The respective reaction product **F** exhibits a similar TG/MS fragmentation behavior as we have observed for reductively activated SWCNT material after aqueous workup (**D**). In both cases, oxygen-containing fragments with m/z 17, 18, and 44 were detected (Figure S20). However, in contrast to **D** no hydrogen signal (m/z 2) was obtained for **F**. The successful introduction of hydroxyl groups by the reaction of uncharged SWCNTs with superoxide anions is also reflected by the respective Raman data (Figure S21). The obtained $I_{D/G}$ value of 0.15 is in the same order of magnitude as the value obtained for the reductively functionalized material $\mathbf{D_2}$.

dx.doi.org/10.1021/ja4063713 | J. Am. Chem. Soc. 2013, 135, 18385−18395

Based on the results of this mechanistic study, the conclusion can be drawn that the reaction of carbon nanotubides with electrophiles does only lead to a partial discharging of the anionic intermediates in the course of the covalent addend binding. The subsequent aqueous work up of the material leads to an additional attachment of hydroxyl groups and protons to the carbon nanotube framework and therefore the generation of mixed functionalized SWCNT derivatives. In order to elaborate alternative routes to monofunctional SWCNT architectures, it is necessary to fully discharge the initially functionalized SWCNT derivatives, without triggering additional chemical functionalization sequences. Inspired by electrochemical-based charging experiments,[60,61] we followed a heterogeneous charge compensation approach by using a platinum gauze as a discharging electrode. After the primary functionalization with *n*-hexyl iodide the SWCNT dispersion was stirred for an additional hour under an argon inert gas atmosphere in the presence of grounded platinum gauze followed by an aqueous work up under ambient conditions. The respective Raman, TG/MS and IR characterization of the charge neutralized material $\mathbf{C}_1^{ac(discharge)}$ is presented in Figure S22. The Raman data (Figure S22a) confirm that the overall degree of functionalization is comparable with the degree of functionalization obtained for the reductively alkylated material $\mathbf{C}_1^{ic}$ ($I_{D/G}$ = 0.55). Nevertheless, as evidenced by the respective Raman histogram, the final bulk material of $\mathbf{C}_1^{ac(discharge)}$ consists of two distinct species with a $I_{D/G}$ value of 0.45 and 0.85, respectively. Therefore, the conclusion can be drawn that the additional functionalization with oxygen and water can partially be suppressed, which is also in total agreement with the data obtained by the respective IR analysis (Figure S22b) and the respective TG/MS data (Figure S22c,d). All these results indicate that the applied charge compensation protocol is a promising approach toward the synthesis of monofunctional SWCNT derivatives, based on reductively activated carbon nanotubide intermediates.

Proposed Mechanism. For the formation of the oxygen-containing byproducts during the aqueous work up of the alkylated carbon nanotubides a possible reaction mechanism based on discrete discharging steps can be discussed (Figure 9).

The reductive alkylation/arylation of negatively charged carbon nanotubides and the diazonium-based arylation of neutral SWCNTs salts is initiated by a single electron transfer processes with the carbon nanotube species as electron donor component (Figure 9, **1** → **2**).[10,25,62−64] Subsequently, the generated alkyl/aryl radicals attack the sp^2 framework. The single electron transfer from the carbon nanotubide intermediates to the electrophile acceptor component is continuously associated with a depopulation of conduction band states. This process depends on the reduction potential of the electrophile and is stopped when the distinct redox potential of the electrophile is reached ($E^\circ \sim -1.7$ V).[65] Therefore, even with an excess of alkyl iodides it is not possible to deplete the conduction bands fully, which means that there are still negatively charged, sidewall functionalized carbon nanotubide derivatives hex_m-SWCNT$^{(n-m)-}$ **2** present in the reaction mixture. In the subsequent aqueous work up, these activated carbon nanotubides can act as electron-donor components in the presence of oxygen (E° = −0.33 V, pH 7)[66] which leads to the formation of a superoxide anion radical (Scheme 3a).

These highly reactive oxygen species can undergo a disproportionation reaction yielding hydrogen peroxide, oxygen and water (Scheme 3b) or can attack the carbon nanotube π-system yielding covalently attached peroxide groups (Scheme 3c). Finally, sidewall hydroxylated SWCNT derivatives can be formed by an intramolecular disproportionation reaction with hydrogen peroxide (Scheme 3d) or by an intra or inter two-electron reduction process in presence the of a proton source (Scheme 3e).

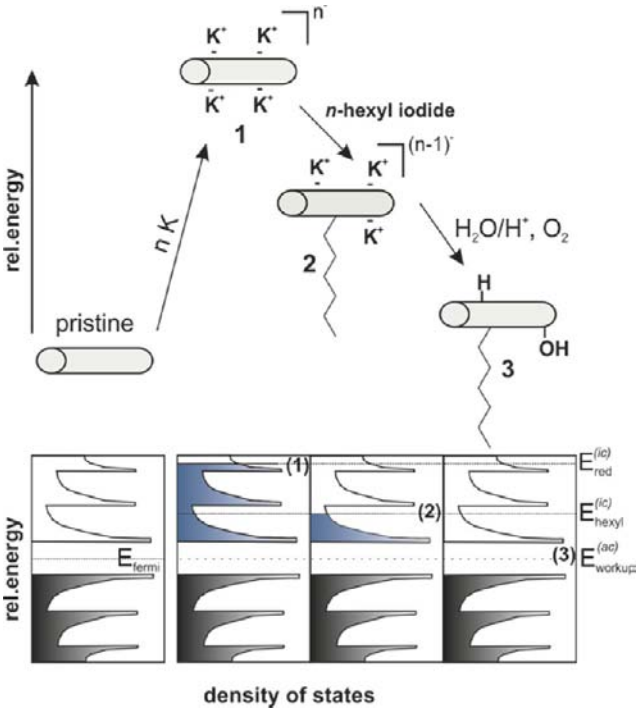

Figure 9. Proposed reaction mechanism for the radical grafting of *n*-hexyl groups at the framework of SWCNTs. Schematic presentation of the stepwise addition reaction. In a first reaction step, *n*-hexyl moieties are attached, followed by a second reaction step leading to the formation of byproducts due to the aqueous work up. The radical addition of *n*-hexyl moieties proceeds, until the redox potential of the SWCNTs matches the redox potential of hexyl iodide. The remaining negative charges on the hexyl functionalized SWCNT intermediates are responsible for the additional sidewall functionalization by O_2/H_2O.

The formation of mixed functionalized SWCNT derivatives of the type (**3**) (Figure 9) with covalently bound hydrogen atoms can also be explained by this radical mechanism. During the aqueous work up H_2O/H^+ can act as an electron-acceptor system (E° = 0 V), yielding hydrogen radicals for a subsequent SWCNT sidewall functionalization reaction. Alternatively, a direct protonation of the charged SWCNT intermediates is also a likely process. This reductive protonation of a carbon framework has recently been observed by Billups[67] and our group[68] investigating the chemical functionalization of graphene.

■ CONCLUSION

In conclusion, we have presented a systematic and careful analysis of carbon nanotubide formation under strict inert conditions followed by the investigation of follow-up reactions with hexyl iodide, moisture (H_2O, O_2), and KO_2. The covalent functionalization of SWCNTs *via* the reaction of the carbon nanotubides with electrophiles belongs to the most important and efficient reactions in nanotube chemistry. The emphasis of this work lies in shining light on the reaction mechanism, the control of the functionalization efficiency, and the detailed

dx.doi.org/10.1021/ja4063713 | J. Am. Chem. Soc. 2013, 135, 18385−18395

Scheme 3. Reductive Hydroxylation and Reductive Protonation of Intermediately Activated Carbon Nanotubides

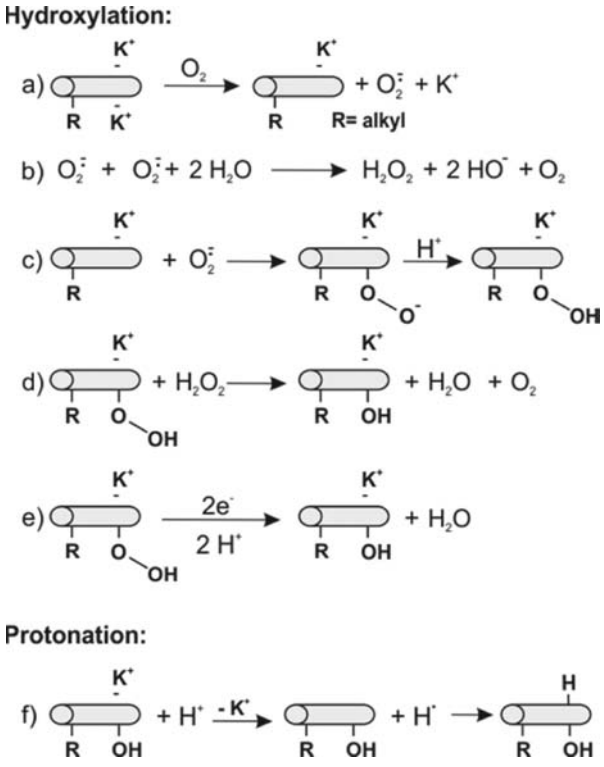

study of the reactivity of the intermediately formed carbon nanotubides with respect to various reaction conditions. We clearly demonstrate that it is very important to work under strict inert gas conditions in order to exclude side reactions. Even after quenching of the nanotubides with hexyl iodide there are still negative charges left, which are very sensitive to moisture and atmospheric oxygen. This leads to the formation of oxygen and hydrogen functionalities in addition to alkyl chain binding. The amount of remaining negative charges on the tubes depends on the reduction potential of the electrophile. This in turn should provide a basis of reaction control by tuning the electronic properties of the electrophilic quenching addend. The particular combination of statistical Raman analysis and other characterization tools together with a systematic variation of the reaction conditions presented in this study provided a deep insight into fundamental aspects of carbon nanotube reactivity, being of great importance for future refinements and for the development of well characterized carbon nanotube derivatives.

■ ASSOCIATED CONTENT

Supporting Information

Experimental details regarding the synthesis of the different SWCNTs derivatives, additional Raman analysis, TG/MS, fluorescence, UV−vis nIR and IR characterization. This material is available free of charge via the Internet at http://pubs.acs.org.

■ AUTHOR INFORMATION

Corresponding Author

andreas.hirsch@fau.de

Notes

The authors declare no competing financial interest.

■ ACKNOWLEDGMENTS

The authors thank the Deutsche Forschungsgemeinschaft (DFG - SFB 953, Project A1 “Synthetic Carbon Allotropes”), the Interdisciplinary Center for Molecular Materials (ICMM), the European Research Council (ERC; grant 246622 GRAPHENOCHEM), the Graduate School Molecular Science (GSMS) and the Cluster of Excellence ‘Engineering of Advanced Materials (EAM)’ for financial support.

■ REFERENCES

(1) Karousis, N.; Tagmatarchis, N.; Tasis, D. *Chem. Rev.* **2010**, *110*, 5366.
(2) Singh, P.; Campidelli, S.; Giordani, S.; Bonifazi, D.; Bianco, A.; Prato, M. *Chem. Soc. Rev.* **2009**, *38*, 2214.
(3) Engel, P. S.; Billups, W. E.; Abmayr, D. W., Jr.; Tsvaygboym, K.; Wang, R. *J. Phys. Chem. C* **2008**, *112*, 695.
(4) Mukherjee, A.; Combs, R.; Chattopadhyay, J.; Abmayr, D. W.; Engel, P. S.; Billups, W. E. *Chem. Mater.* **2008**, *20*, 7339.
(5) Hamilton, C. E.; Lomeda, J. R.; Sun, Z.; Tour, J. M.; Barron, A. R. *Nano Res.* **2010**, *3*, 138.
(6) Gebhardt, B.; Syrgiannis, Z.; Backes, C.; Graupner, R.; Hauke, F.; Hirsch, A. *J. Am. Chem. Soc.* **2011**, *133*, 7985.
(7) Gebhardt, B.; Hof, F.; Backes, C.; Mueller, M.; Plocke, T.; Maultzsch, J.; Thomsen, C.; Hauke, F.; Hirsch, A. *J. Am. Chem. Soc.* **2011**, *133*, 19459.
(8) Hodge, S. A.; Bayazit, M. K.; Coleman, K. S.; Shaffer, M. S. P. *Chem. Soc. Rev.* **2012**, *41*, 4409.
(9) Syrgiannis, Z.; Gebhardt, B.; Dotzer, C.; Hauke, F.; Graupner, R.; Hirsch, A. *Angew. Chem., Int. Ed.* **2010**, *49*, 3322.
(10) Chattopadhyay, J.; Chakraborty, S.; Mukherjee, A.; Wang, R.; Engel, P. S.; Billups, W. E. *J. Phys. Chem. C* **2007**, *111*, 17928.
(11) Liang, F.; Beach, J. M.; Kobashi, K.; Sadana, A. K.; Vega-Cantu, Y. I.; Tour, J. M.; Billups, W. E. *Chem. Mater.* **2006**, *18*, 4764.
(12) Voiry, D.; Roubeau, O.; Pénicaud, A. *J. Mater. Chem.* **2010**, *20*, 4385.
(13) Dresselhaus, M. S.; Dresselhaus, G. *Adv. Phys.* **1981**, *30*, 139.
(14) Akuzawa, N.; Fujisawa, T.; Amemiya, T.; Takahashi, Y. *Synth. Met.* **1983**, *7*, 57.
(15) Rüdorff, W. *Angew. Chem.* **1959**, *71*, 487.
(16) Fredenhagen, K.; Cadenbach, G. *Z. Anorg. Allg. Chem.* **1926**, *158*, 249.
(17) Englert, J. M.; Dotzer, C.; Yang, G.; Schmid, M.; Papp, C.; Gottfried, J. M.; Steinruck, H.-P.; Spiecker, E.; Hauke, F.; Hirsch, A. *Nat. Chem.* **2011**, *3*, 279.
(18) Benning, P. J.; Poirier, D. M.; Ohno, T. R.; Chen, Y.; Jost, M. B.; Stepniak, F.; Kroll, G. H.; Weaver, J. H.; Fure, J.; Smalley, R. E. *Phys. Rev. B* **1992**, *45*, 6899.
(19) Martins, J. L.; Troullier, N. *Phys. Rev. B* **1992**, *46*, 1766.
(20) Hebard, A. F.; Rosseinsky, M. J.; Haddon, R. C.; Murphy, D. W.; Glarum, S. H.; Palstra, T. T. M.; Ramirez, A. P.; Kortan, A. R. *Nature* **1991**, *350*, 600.
(21) Allemand, P.-M.; Khemani, K. C.; Koch, A.; Wudl, F.; Holczer, K.; Donovan, S.; Grüner, G.; Thompsen, J. D. *Science* **1991**, *253*, 301.
(22) Viswanathan, G.; Chakrapani, N.; Yang, H.; Wei, B.; Chung, H.; Cho, K.; Ryu, C. Y.; Ajayan, P. M. *J. Am. Chem. Soc.* **2003**, *125*, 9258.
(23) Wunderlich, D.; Hauke, F.; Hirsch, A. *Chem.—Eur. J.* **2008**, *14*, 1607.
(24) Wunderlich, D.; Hauke, F.; Hirsch, A. *J. Mater. Chem.* **2008**, *18*, 1493.
(25) Strano, M. S.; Dyke, C. A.; Usrey, M. L.; Barone, P. W.; Allen, M. J.; Shan, H.; Kittrell, C.; Hauge, R. H.; Tour, J. M.; Smalley, R. E. *Science* **2003**, *301*, 1519.
(26) Liang, F.; Sadana, A. K.; Peera, A.; Chattopadhyay, J.; Gu, Z.; Hauge, R. H.; Billups, W. E. *Nano Lett.* **2004**, *4*, 1257.

(27) Chattopadhyay, J.; Sadana, A. K.; Liang, F.; Beach, J. M.; Xiao, Y.; Hauge, R. H.; Billups, W. E. *Org. Lett.* **2005**, *7*, 4067.
(28) Pénicaud, A.; Poulin, P.; Derré, A.; Anglaret, E.; Petit, P. *J. Am. Chem. Soc.* **2005**, *127*, 8.
(29) Fogden, S.; Howard, C. A.; Heenan, R. K.; Skipper, N. T.; Shaffer, M. S. P. *ACS Nano* **2011**, *6*, 54.
(30) Voiry, D.; Vallés, C.; Roubeau, O.; Pénicaud, A. *Carbon* **2011**, *49*, 170.
(31) Paolucci, D.; Franco, M. M.; Iurlo, M.; Marcaccio, M.; Prato, M.; Zerbetto, F.; Pénicaud, A.; Paolucci, F. *J. Am. Chem. Soc.* **2008**, *130*, 7393.
(32) Hilmer, A. J.; McNicholas, T. P.; Lin, S.; Zhang, J.; Wang, Q. H.; Mendenhall, J. D.; Song, C.; Heller, D. A.; Barone, P. W.; Blankschtein, D.; Strano, M. S. *Langmuir* **2011**, *28*, 1309.
(33) Hof, F.; Bosch, S.; Englert, J. M.; Hauke, F.; Hirsch, A. *Angew. Chem., Int. Ed.* **2012**, *51*, 11727.
(34) Hansson, A.; Stafström, S. *Phys. Rev. B* **2005**, *72*, 125420.
(35) Chen, G.; Furtado, C. A.; Bandow, S.; Iijima, S.; Eklund, P. C. *Phys. Rev. B* **2005**, *71*, 045408.
(36) Fischer, J. E. *Acc. Chem. Res.* **2002**, *35*, 1079.
(37) Tanaka, Y.; Hirana, Y.; Niidome, Y.; Kato, K.; Saito, S.; Nakashima, N. *Angew. Chem., Int. Ed.* **2009**, *48*, 7655.
(38) Park, J. S.; Hirana, Y.; Mouri, S.; Miyauchi, Y.; Nakashima, N.; Matsuda, K. *J. Am. Chem. Soc.* **2012**, *134*, 14461.
(39) Kim, S. M.; Kim, K. K.; Duong, D. L.; Hirana, Y.; Tanaka, Y.; Niidome, Y.; Nakashima, N.; Kong, J.; Lee, Y. H. *J. Phys. Chem. C* **2012**, *116*, 5444.
(40) Bendiab, N.; Righi, A.; Anglaret, E.; Sauvajol, J. L.; Duclaux, L.; Béguin, F. *Chem. Phys. Lett.* **2001**, *339*, 305.
(41) Dragin, F.; Pénicaud, A.; Iurlo, M.; Marcaccio, M.; Paolucci, F.; Anglaret, E.; Martel, R. *ACS Nano* **2011**, *5*, 9892.
(42) Akdim, B.; Duan, X.; Shiffler, D. A.; Pachter, R. *Phys. Rev. B* **2005**, *72*, 121402.
(43) Rauf, H.; Pichler, T.; Knupfer, M.; Fink, J.; Kataura, H. *Phys. Rev. Lett.* **2004**, *93*, 096805.
(44) Duclaux, L.; Salvetat, J. P.; Lauginie, P.; Cacciaguera, T.; Faugère, A. M.; Goze-Bac, C.; Bernier, P. *J. Phys. chem. Solids* **2003**, *64*, 571.
(45) Duclaux, L. *Carbon* **2002**, *40*, 1751.
(46) Claye, A.; Rahman, S.; Fischer, J. E.; Sirenko, A.; Sumanasekera, G. U.; Eklund, P. C. *J. Phys., Lett.* **2001**, *333*, 16.
(47) Claye, A. S.; Nemes, N. M.; Jánossy, A.; Fischer, J. E. *Phys. Rev. B* **2000**, *62*, R4845.
(48) Gao, G.; Çağin, T.; Goddard, W. A., III *Phys. Rev. Lett.* **1998**, *80*, 5556.
(49) Miyamoto, Y.; Rubio, A.; Blase, X.; Cohen, M. L.; Louie, S. G. *Phys. Rev. Lett.* **1995**, *74*, 2993.
(50) Rao, A. M.; Eklund, P. C.; Bandow, S.; Thess, A.; Smalley, R. E. *Nature* **1997**, *388*, 257.
(51) Kalbac, M.; Kavan, L. *J. Phys. Chem. C* **2009**, *113*, 16408.
(52) Guan, J.; Martinez-Rubi, Y.; Dénommée, S.; Ruth, D.; Kingston, C. T.; Daroszewska, M.; Barnes, M.; Simard, B. *Nanotechnology* **2009**, *20*, 245701.
(53) Raravikar, N. R.; Keblinski, P.; Rao, A. M.; Dresselhaus, M. S.; Schadler, L. S.; Ajayan, P. M. *Phys. Rev. B* **2002**, *66*, 235424.
(54) Dreyer, D. R.; Park, S.; Bielawski, C. W.; Ruoff, R. S. *Chem. Soc. Rev.* **2010**, *39*, 228.
(55) Gao, X.; Jang, J.; Nagase, S. *J. Phys. Chem. C* **2009**, *114*, 832.
(56) Cui, P.; Lee, J.; Hwang, E.; Lee, H. *Chem. Commun.* **2011**, *47*, 12370.
(57) Begović, N.; Marković, Z.; Anić, S.; Kolar-Anić, L. *J. Phys. Chem. A* **2004**, *108*, 651.
(58) Phillips, B. A.; Busing, W. R. *J. Phys. Chem.* **1957**, *61*, 502.
(59) Miller, F. A.; Wilkins, C. H. *Anal. Chem.* **1952**, *24*, 1253.
(60) Hodge, S. A.; Fogden, S.; Howard, C. A.; Skipper, N. T.; Shaffer, M. S. P. *ACS Nano* **2013**, *7*, 1769.
(61) Jiang, C.; Saha, A.; Xiang, C.; Young, C. C.; Tour, J. M.; Pasquali, M.; Martí, A. A. *ACS Nano* **2013**, *7*, 4503.
(62) Usrey, M. L.; Lippmann, E. S.; Strano, M. S. *J. Am. Chem. Soc.* **2005**, *127*, 16129.
(63) Schmidt, G.; Gallon, S.; Esnouf, S.; Bourgoin, J.-P.; Chenevier, P. *Chem.—Eur. J.* **2009**, *15*, 2101.
(64) Ramirez, J.; Mayo, M. L.; Kilina, S.; Tretiak, S. *Chem. Phys.* **2013**, *413*, 89.
(65) Occhialini, D.; Pedersen, S. U.; Lund, H. *Acta Chem. Scan.* **1990**, *44*, 715.
(66) Wood, P. M. *Bichem. J.* **1988**, *253*, 287.
(67) Yang, Z.; Sun, Y.; Alemany, L. B.; Narayanan, T. N.; Billups, W. E. *J. Am. Chem. Soc.* **2012**, *134*, 18689.
(68) Schäfer, R. A.; Englert, J. M.; Wehrfritz, P.; Bauer, W.; Hauke, F.; Seyller, T.; Hirsch, A. *Angew. Chem., Int. Ed.* **2013**, *52*, 754.